Real-time endoscopic optical properties imaging.

Joseph Angelo, Martijn van de Giessen, Sylvain Gioux

▶ **To cite this version:**

Joseph Angelo, Martijn van de Giessen, Sylvain Gioux. Real-time endoscopic optical properties imaging.. Biomedical optics express, 2017, 8 (11), pp.5113-5126. 10.1364/BOE.8.005113 . hal-01878616

HAL Id: hal-01878616
https://hal.science/hal-01878616

Submitted on 11 Oct 2018

HAL is a multi-disciplinary open access archive for the deposit and dissemination of scientific research documents, whether they are published or not. The documents may come from teaching and research institutions in France or abroad, or from public or private research centers.

L'archive ouverte pluridisciplinaire **HAL**, est destinée au dépôt et à la diffusion de documents scientifiques de niveau recherche, publiés ou non, émanant des établissements d'enseignement et de recherche français ou étrangers, des laboratoires publics ou privés.

Research Article | Vol. 8, No. 11 | 1 Nov 2017 | BIOMEDICAL OPTICS EXPRESS 5113
Biomedical Optics EXPRESS

Real-time endoscopic optical properties imaging

JOSEPH P. ANGELO,[1,2] MARTIJN VAN DE GIESSEN,[3] AND SYLVAIN GIOUX[4,5,*]

[1]Department of Medicine, Beth Israel Deaconess Medical Center, Boston, MA 02215, USA
[2]Department of Biomedical Engineering Boston University, Boston, MA 02215, USA
[3]Department of Radiology, Leiden University Medical Center, Leiden, The Netherlands
[4]Department of Surgery, Beth Israel Deaconess Medical Center, Boston, MA 02215, USA
[5]ICube Laboratory, University of Strasbourg, 300 Bd S. Brant, Illkirch, 67412 France
*sgioux@unistra.fr

Abstract: With almost 50% of all surgeries in the U.S. being performed as minimally invasive procedures, there is a need to develop quantitative endoscopic imaging techniques to aid surgical guidance. Recent developments in widefield optical imaging make endoscopic implementations of real-time measurement possible. In this work, we introduce a proof-of-concept endoscopic implementation of a functional widefield imaging technique called 3D single snapshot of optical properties (3D-SSOP) that provides quantitative maps of absorption and reduced scattering optical properties as well as surface topography with simple instrumentation added to a commercial endoscope. The system's precision and accuracy is validated using tissue-mimicking phantoms, showing a max error of 0.004 mm^{-1}, 0.05 mm^{-1}, and 1.1 mm for absorption, reduced scattering, and sample topography, respectively. This study further demonstrates video acquisition of a moving phantom and an *in vivo* sample with a framerate of approximately 11 frames per second.

© 2017 Optical Society of America

OCIS codes: (170.0170) Medical optics and biotechnology; (170.0110) Imaging systems; (170.2150) Endoscopic imaging

References and links

1. C. Tsui, R. Klein, and M. Garabrant, "Minimally invasive surgery: national trends in adoption and future directions for hospital strategy," Surg. Endosc. **27**(7), 2253–2257 (2013).
2. J. Fengler, "Near-infrared fluorescence laparoscopy-technical description of PINPOINT(R) a novel and commercially available system," Colorectal Dis. **17**(Suppl 3), 3–6 (2015).
3. N. Thekkek, M. H. Lee, A. D. Polydorides, D. G. Rosen, S. Anandasabapathy, and R. Richards-Kortum, "Quantitative evaluation of in vivo vital-dye fluorescence endoscopic imaging for the detection of Barrett's-associated neoplasia," J. Biomed. Opt. **20**(5), 56002 (2015).
4. Y. Jiang, Y. Gong, J. H. Rubenstein, T. D. Wang, and E. J. Seibel, "Toward real-time quantification of fluorescence molecular probes using target/background ratio for guiding biopsy and endoscopic therapy of esophageal neoplasia," J. Med. Imaging (Bellingham) **4**(2), 024502 (2017).
5. R. Leitner, M. De Biasio, T. Arnold, C. V. Dinh, M. Loog, and R. P. Duin, "Multi-spectral video endoscopy system for the detection of cancerous tissue," Pattern Recognit. Lett. **34**, 85–93 (2013).
6. N. Bodenschatz, S. Lam, A. Carraro, J. Korbelik, D. M. Miller, J. N. McAlpine, M. Lee, A. Kienle, and C. MacAulay, "Diffuse optical microscopy for quantification of depth-dependent epithelial backscattering in the cervix," J. Biomed. Opt. **21**(6), 66001 (2016).
7. T. Rath, G. E. Tontini, M. Vieth, A. Nägel, M. F. Neurath, and H. Neumann, "In vivo real-time assessment of colorectal polyp histology using an optical biopsy forceps system based on laser-induced fluorescence spectroscopy," Endoscopy **48**(6), 557–562 (2016).
8. N. J. Durr, V. Parot, G. Traverso, W. P. Puricelli, B. J. Vakoc, N. S. Nishioka, and G. Gonzalez, "Imaging colonic surface topography with a photometric stereo endoscope," Gastrointest. Endosc. **79**, 5S (2014).
9. I. Intuitive Surgical, "Da Vinci Surgical System" (Intuitive Surgical, Inc.), retrieved August, 2016, *http://www.intuitivesurgical.com*.
10. I. Olympus, "Endoeye Flex 3D" (Olympus, Inc), retrieved August, 2016, medical.olympusamerica.com.
11. J. Vervandier and S. Gioux, "Single snapshot imaging of optical properties," Biomed. Opt. Express **4**(12), 2938–2944 (2013).

#306171 https://doi.org/10.1364/BOE.8.005113
Journal © 2017 Received 7 Sep 2017; revised 11 Oct 2017; accepted 11 Oct 2017; published 19 Oct 2017

Biomedical Optics EXPRESS

12. K. P. Nadeau, A. J. Durkin, and B. J. Tromberg, "Advanced demodulation technique for the extraction of tissue optical properties and structural orientation contrast in the spatial frequency domain," J. Biomed. Opt. **19**(5), 056013 (2014).
13. N. Dögnitz and G. Wagnières, "Determination of tissue optical properties by steady-state spatial frequency-domain reflectometry," Lasers Med. Sci. **13**, 55–65 (1998).
14. D. J. Cuccia, F. Bevilacqua, A. J. Durkin, and B. J. Tromberg, "Modulated imaging: quantitative analysis and tomography of turbid media in the spatial-frequency domain," Opt. Lett. **30**(11), 1354–1356 (2005).
15. D. J. Cuccia, F. Bevilacqua, A. J. Durkin, F. R. Ayers, and B. J. Tromberg, "Quantitation and mapping of tissue optical properties using modulated imaging," J. Biomed. Opt. **14**(2), 024012 (2009).
16. S. Gioux, A. Mazhar, D. J. Cuccia, A. J. Durkin, B. J. Tromberg, and J. V. Frangioni, "Three-dimensional surface profile intensity correction for spatially modulated imaging," J. Biomed. Opt. **14**(3), 034045 (2009).
17. Y. Zhao, S. Tabassum, S. Piracha, M. S. Nandhu, M. Viapiano, and D. Roblyer, "Angle correction for small animal tumor imaging with spatial frequency domain imaging (SFDI)," Biomed. Opt. Express **7**(6), 2373–2384 (2016).
18. A. Mazhar, S. Dell, D. J. Cuccia, S. Gioux, A. J. Durkin, J. V. Frangioni, and B. J. Tromberg, "Wavelength optimization for rapid chromophore mapping using spatial frequency domain imaging," J. Biomed. Opt. **15**(6), 061716 (2010).
19. S. Gioux, A. Mazhar, B. T. Lee, S. J. Lin, A. M. Tobias, D. J. Cuccia, A. Stockdale, R. Oketokoun, Y. Ashitate, E. Kelly, M. Weinmann, N. J. Durr, L. A. Moffitt, A. J. Durkin, B. J. Tromberg, and J. V. Frangioni, "First-in-human pilot study of a spatial frequency domain oxygenation imaging system," J. Biomed. Opt. **16**(8), 086015 (2011).
20. M. van de Giessen, J. P. Angelo, and S. Gioux, "Real-time, profile-corrected single snapshot imaging of optical properties," Biomed. Opt. Express **6**(10), 4051–4062 (2015).
21. K. P. Nadeau, T. B. Rice, A. J. Durkin, and B. J. Tromberg, "Multifrequency synthesis and extraction using square wave projection patterns for quantitative tissue imaging," J. Biomed. Opt. **20**(11), 116005 (2015).
22. T. J. Farrell, M. S. Patterson, and B. Wilson, "A diffusion theory model of spatially resolved, steady-state diffuse reflectance for the noninvasive determination of tissue optical properties in vivo," Med. Phys. **19**(4), 879–888 (1992).
23. V. Venugopal, M. Park, Y. Ashitate, F. Neacsu, F. Kettenring, J. V. Frangioni, S. P. Gangadharan, and S. Gioux, "Design and characterization of an optimized simultaneous color and near-infrared fluorescence rigid endoscopic imaging system," J. Biomed. Opt. **18**(12), 126018 (2013).
24. M. Takeda and K. Mutoh, "Fourier transform profilometry for the automatic measurement of 3-D object shapes," Appl. Opt. **22**(24), 3977 (1983).
25. W. S. Zhou and X. Y. Su, "A Direct Mapping Algorithm for Phase-measuring Profilometry," J. Mod. Opt. **41**, 89–94 (1994).
26. J. Swartling, A. Pifferi, A. M. Enejder, and S. Andersson-Engels, "Accelerated Monte Carlo models to simulate fluorescence spectra from layered tissues," J. Opt. Soc. Am. A **20**(4), 714–727 (2003).
27. F. Ayers, A. Grant, D. Kuo, D. J. Cuccia, and A. J. Durkin, "Fabrication and characterization of silicone-based tissue phantoms with tunable optical properties in the visible and near infrared domain," in 2008), 687007–687009.
28. T. H. Pham, F. Bevilacqua, T. Spott, J. S. Dam, B. J. Tromberg, and S. Andersson-Engels, "Quantifying the absorption and reduced scattering coefficients of tissuelike turbid media over a broad spectral range with noncontact Fourier-transform hyperspectral imaging," Appl. Opt. **39**(34), 6487–6497 (2000).
29. M. Ghijsen, B. Choi, A. J. Durkin, S. Gioux, and B. J. Tromberg, "Real-time simultaneous single snapshot of optical properties and blood flow using coherent spatial frequency domain imaging (cSFDI)," Biomed. Opt. Express **7**(3), 870–882 (2016).
30. P. Diep, S. Pannem, J. Sweer, J. Lo, M. Snyder, G. Stueber, Y. Zhao, S. Tabassum, R. Istfan, J. Wu, S. Erramilli, and D. Roblyer, "Three-dimensional printed optical phantoms with customized absorption and scattering properties," Biomed. Opt. Express **6**(11), 4212–4220 (2015).
31. J. Angelo, C. R. Vargas, B. T. Lee, I. J. Bigio, and S. Gioux, "Ultrafast optical property map generation using lookup tables," J. Biomed. Opt. **21**(11), 110501 (2016).
32. P. A. Valdes, J. P. Angelo, H. S. Choi, and S. Gioux, "qF-SSOP: real-time optical property corrected fluorescence imaging," Biomed. Opt. Express **8**(8), 3597–3605 (2017).
33. M. Sibai, I. Veilleux, J. T. Elliott, F. Leblond, and B. C. Wilson, "Quantitative spatial frequency fluorescence imaging in the sub-diffusive domain for image-guided glioma resection," Biomed. Opt. Express **6**(12), 4923–4933 (2015).
34. K. P. Nadeau, A. Ponticorvo, H. J. Lee, D. Lu, A. J. Durkin, and B. J. Tromberg, "Quantitative assessment of renal arterial occlusion in a porcine model using spatial frequency domain imaging," Opt. Lett. **38**(18), 3566–3569 (2013).

1. Introduction

With the rapid increase in the number of minimally invasive procedures aimed at improving patient care while lowering the healthcare financial burden [1], there has been a strong push for optical technologies to provide clinicians guidance during endoscopic procedures. This

Biomedical Optics EXPRESS

need for guidance is clearly evidenced by the development of instruments by both investigators and companies that aim at aiding visualization using techniques such as fluorescence [2–4], endogenous imaging [5–7], and stereoscopic imaging [8–10]. Unfortunately, most of these techniques are not quantitative in nature and are therefore subject to interpretation and user experience, limiting their value for being used routinely in clinical settings. With point measurements methods having established the potential of quantitative optical measurements for providing high sensitivity and specificity in many diseases and conditions, it is of paramount importance to develop novel methods and instruments that would allow real-time optical quantitative imaging through endoscopes.

Spatial frequency domain imaging (SFDI) has recently been pushed to real-time acquisition [11, 12] and is particularly well-suited for endoscopic implementation. SFDI offers a widefield, noncontact approach for acquiring optical property maps that can be analyzed over several wavelengths to produce chromophore concentrations of endogenous tissue constituents [13–15]. Several steps have been made to improve the technique's robustness and processing schemes, including a fast 2-D look-up Table [15], a 3-D height correction method [16, 17], and an optimization of wavelengths for spectroscopic fitting of tissue constituent concentrations [18]. These developments led to a first-in-human pilot study that measured skin flap oxygenation during reconstructive breast surgery [19]. However, further work was needed in order to avoid motion artifacts and to approach real-time image acquisition for image-guided surgery.

Recent developments have pushed the speed of SFDI, reducing its usual requirement of 6 image acquisitions down to two [12] and even to one by using single snapshot of optical properties (SSOP) processing [11]. The single exposure acquisition and simple instrumentation of SSOP makes it amenable to the demanding environment of endoscopic imaging. Moreover, recent work has demonstrated the ability to extract phase information from a single projection while using SSOP, enabling height-corrections that accommodate for irradiance loss due to variations in surface topography [20]. These features have led to this study that aims to provide quantitative endoscopic imaging.

All previously reported techniques using spatial frequency domain analysis have relied on the concept of constant, known frequency projection. Analysis of at least two frequencies (AC and DC) is required, though multi-frequency has long been studied [15]. However, because each spatial frequency that is projected must be known, projection is approximated as telecentric such that the projected pattern spatial frequency is assumed to be constant over depth and across the field of view, and analysis is applied uniformly across the acquired images. If multiple frequencies are acquired in a single image [11, 21], these assumptions are still made. The nature of endoscopic imaging requires a new perspective for spatial frequency processing.

Endoscopes are commonly made such that the angular field of view is constant, allowing practitioners a magnified view when the endoscope is close to the sample and a broad field of view when the sample is distant. Hence, in order to practically enable endoscopic SFDI, a projection pattern must come from the endoscope itself and follow the same angular field of view. This implies a highly divergent illumination pattern, meaning the projected frequency at every pixel will vary with distance from the endoscope. Herein, we stray from the above assumptions of pattern projection and employ a novel spatial-frequency calibration based on sample depth along with an n-dimensional lookup table (nD-LUT).

The work presented in this article utilizes the state of the art in SFDI acquisition techniques and further advances the field by introducing methodologies for high NA pattern projection and image collection. Furthermore, these developments permit, for the first time, a proof-of-concept endoscopic implementation of a functional widefield imaging technique that provides quantitative maps of absorption and reduced scattering optical properties as well as surface topography in real-time. SSOP acquisition and processing is utilized for speed and simplicity of instrumentation along with SFDI calibration and modeling for robust

Biomedical Optics EXPRESS

quantitative measurement. This study validates the developed system to accurately and precisely measure optical properties and height maps of tissue-mimicking phantoms and further demonstrates video acquisition of a moving phantom and an *in vivo* sample.

2. Materials and methods

2.1 Spatial frequency domain imaging

Spatial frequency domain imaging (SFDI) has been widely discussed in the literature and so will only be briefly introduced here. It is well known that the spatial response of a point source of light in turbid media can be described by a point spread function, s-PSF, which depends on the subsurface optical properties and radial distance from the source [22]. SFDI uses the medium's calibrated response to spatially modulated light to obtain the spatial modulation transfer function, s-MTF, the Fourier domain equivalent of the s-PSF. The s-MTF is obtained through the analysis of the diffuse reflectance R_d measured from an intensity sinewave projection. Solving the inverse problem at each image pixel enables spatially resolved mapping of the medium's absorption and reduced scattering properties [13, 14].

This work utilizes the fundamentals of SFDI to acquire and process R_d measurements in the spatial frequency domain, thereby enabling optical property measurements. In practice, the intensity I of a sinusoidal wave at location x and spatial frequency f_x is a linear combination of both an AC signal and a DC offset (we cannot project a negative intensity):

$$I(x, f_x) = I_{DC} + M(x, f_x) \cdot \cos(2\pi f_x \cdot x + \phi) \quad (1)$$

where I_{DC} is the DC offset and $M(x, f_x)$ is the modulation amplitude of the AC signal, and φ is the phase. The modulation amplitude $M(x, f_x)$ can be obtained through various demodulation techniques, and though our work utilizes Fourier demodulation method, the most widely used method for SFDI is a three-phase demodulation where three sequentially projected sinusoidal waves with varying phase φ are acquired in order to isolate the contribution of $M(x, f_x)$ in $I(x, f_x)$. $M(x, f_x)$ is directly related to the sample's diffuse reflectance R_d by

$$M(x, f_x) = I_0 \cdot MTF_{sys}(x, f_x) \cdot R_d(x, f_x) \quad (2)$$

with I_0 as the source intensity and MTF_{sys} as the modulation transform of the optical system. In order to isolate R_d, a calibration measurement is made on a reference phantom with known optical properties (and therefore known R_d) to account for both I_0 and MTF_{sys}. Spatial frequency domain measurements, as opposed to other spatially resolved measurements, have the advantageous multiplicative nature of system frequency response contributions, and these terms are accounted for with a simple division-based correction:

$$R_d(x, f_x) = \frac{M(x, f_x)}{M_{ref}(x, f_x)} \cdot R_{d,ref,pred}(x, f_x) \quad (3)$$

where $M_{ref}(x, f_x)$ is the reference phantom's modulation amplitude and $R_{d,\,ref,\,pred}$ is a model prediction of the reference phantom's diffuse reflectance. One can see that this assumes each measurement has the same source intensity and collection efficiency, and so the reference phantom should ideally have the same surface height and profile as the sample. Otherwise, a profile correction technique should be used to ensure measurement accuracy (discussed below in section 2.3).

Once the R_d of a sample is known, we utilize a model based 2-D look-up table method that can generate optical property maps given the R_d at a minimum of two spatial frequencies, a DC (planar illumination, $f_x = 0$) and an AC measurement, the latter typically around $f_x = 0.15 – 0.2$ mm^{-1} for skin [15]. This modest requirement of the R_{d_DC} and R_{d_AC} measurements enables the use of single snapshot of optical properties imaging, a video-rate acquisition technique in the spatial frequency domain.

Biomedical Optics EXPRESS

2.2 Single snapshot of optical properties imaging

Our lab recently developed a novel spatial frequency domain technique called single snapshot of optical properties (SSOP) that allows for video-rate acquisition of optical properties [11, 20]. Long acquisition times (fewer than 1 frame per second, fps) are prone to motion artifacts created by a moving sample and are unable to capture dynamics of motion or changing optical properties. Long acquisition times are also not suitable for endoscopy, which requires at least a rate of 10 fps for proper visualization [23]. SSOP uses spatial-frequency filtering to demodulate the optical reflectance signal from the projected carrier wave by utilizing the AC and DC components of a single sinusoidal projection. This minimizes the acquisition time to the length of a single exposure, which is simply limited by optical throughput and collection efficiency.

In this work we utilize the line-by-line Fourier transform method originally presented in 2013 [11]. After the 1-D Fourier transform is performed line-by-line over the entire raw image, an ideal frequency filter separates the DC and AC components of the Fourier image. A simple inverse Fourier transform of the DC spectrum recovers the DC image. Single sideband demodulation is performed on the AC image to remove the carrier frequency and recover the AC response image. These DC and AC images correspond to the components of the signal in Eq. (1) and, once calibrated using Eq. (3), provide the R_{d_DC} and R_{d_AC} components needed to utilize a 2-D look-up table and generate optical property maps.

2.3 Endoscopic SSOP

It is often difficult to control the surface height and profile of a sample, and so a profile-correction method was developed by utilizing the distance-dependent phase-shifting behavior of angled sinusoidal projections [16]. Profile corrections are absolutely crucial for both SFDI [16, 17] and SSOP [20] as varying sample height causes uncorrected measurements of absorption and reduced scattering properties. Hence, this work also implements and demonstrates the need for a height-based correction. Note: in an endoscope geometry, it seems more intuitive to describe the sample's position as an absolute measure in space in terms of distance from the endoscope as opposed to a height from an arbitrary ground.

With our endoscope implementation, several parameters of a given measurement change along with the sample's distance from the endoscope, e.g. projected spatial frequency and the radiance of source intensity. However, each of these parameters can be calibrated and accounted for over a range of distances by using the same principles demonstrated previously [16, 20]. For any given parameter, calibration measurements on a reference phantom are made at several known distances from the endoscope and the parameter is fit to a regression as a function of distance. Then, for any given sample distance, this parameter is known and can be corrected. First, the sample's distance from the endoscope must be measured.

The data flow for calibration and sample processing is depicted in Fig. 1. This work utilizes a Fourier transform profilometry technique to measure the sample's surface topography. Using the same fringe pattern for both profilometry and SSOP, the phase of a sample is measured using 1-D line-by-line Fourier processing previously demonstrated [24]. Once the phase is measured for the reference phantom at several known distances, a phase relationship is made and can be utilized for a sample of unknown distance [25]. Therefore, a phase measurement is simultaneously taken for every pixel of a sample, and for every pixel a distance is calculated. This distance measurement is used for intensity corrections as previously demonstrated [16], yet endoscopic SSOP also requires careful consideration of frequency analysis.

Each factor considered in calculating R_d as seen in Eq. (3) depends on the spatial frequency f_x. Calibration for endoscopic SSOP entails creating a regression for projected spatial frequency, as shown in Fig. 1. Once the sample distance is measured, a spatial frequency map is created for the entire image. Before measurements are acquired, limits for the maximum and minimum distances are determined and the range of corresponding spatial

Biomedical Optics EXPRESS

frequencies are split into n bins. A "white" Monte Carlo model [26] is used to generate an n-dimensional lookup table (nD-LUT) and to pre-compute $R_{d,\ ref,\ pred}$ for each frequency bin. Finally, the sample's spatial frequency map separates each pixel into a frequency bin, each spatial frequency bin is processed using the nD-LUT, and optical property maps are generated.

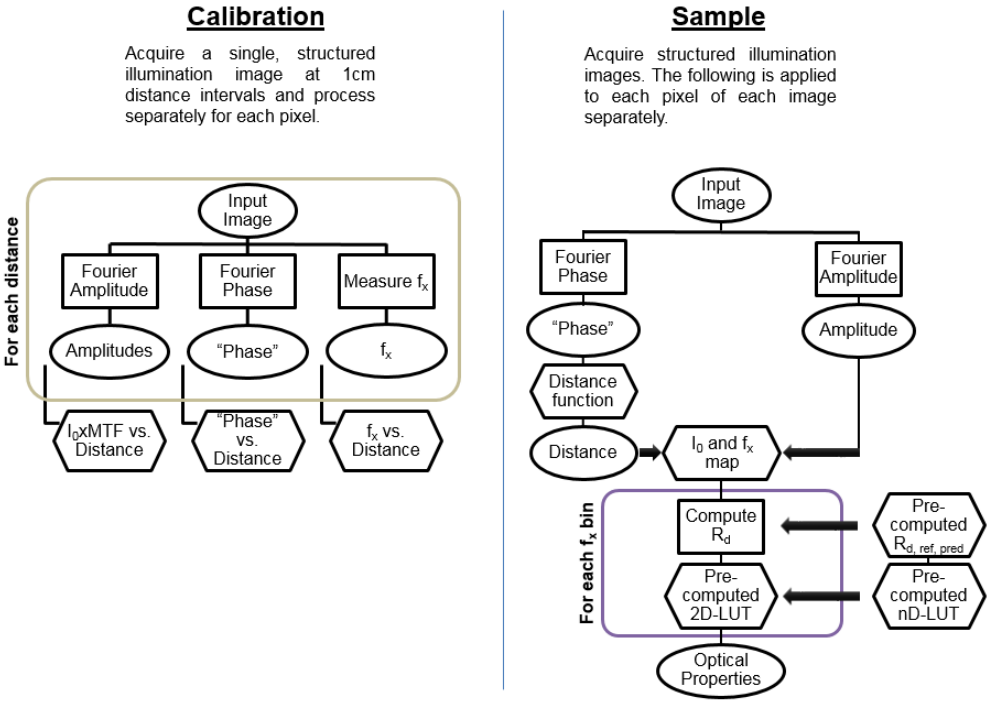

Fig. 1. A data flow schematic for calibration and sample processing using endoscopic SSOP.

2.4 System design

Figure 2(a) depicts the optical design of the endoscopic imaging system. The fundamentals of imaging in the spatial frequency domain are preserved, starting with a light source. Given a source with a fiber output, lenses L_1 and L_2 are used to expand and collimate the beam onto mask M of a sinusoidal pattern. Since SSOP only requires a single pattern, the need for a DMD or other type of variable projector can be replaced by a simple mask. The image of the illuminated pattern is then collimated by L_3 and polarized by linear polarizer P_1 as it is sent through the projection channel of the endoscope and onto the sample. The reflected light is imaged through the collection channel of the endoscope. The collimated output is cross-polarized with respect to P_1 by linear polarizer P_2 and then imaged by objective lens L_4 onto the CCD. The entire endoscope is shown in Fig. 2(b), while the optical channels of the working end of the endoscope are shown in Fig. 2(c).

Biomedical Optics EXPRESS

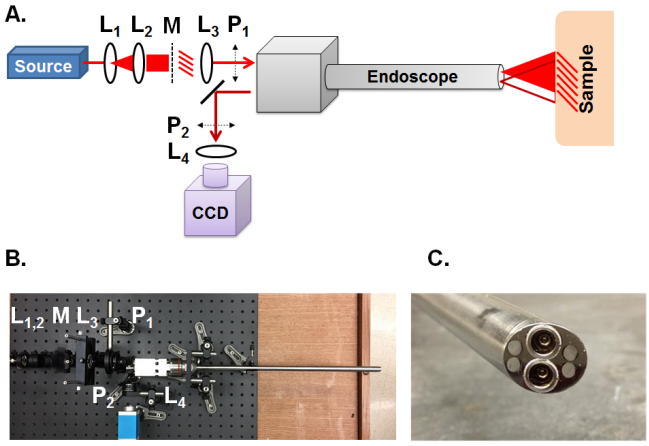

Fig. 2. (a) A schematic of the optical system: a laser source is expanded and collimated by lenses L_1 and L_2, passes through a mask of a sinusoid printed onto a transparency and is collimated by L_3 into the projection channel of the endoscope. The polarizers P_1 and P_2 ensure specular light removal. The collection channel of the endoscope sends light through L_4 where it is imaged onto a CCD camera. (b) A photograph of the optical system. (c) The distal end of the endoscope showing the projection and collection channels.

Figure 3 compares the projection characteristics of (a) standard widefield structured illumination with (b) endoscopic structured illumination used in this work. Both systems have an image projection that undergoes a phase shift as a function of distance from the projector. While widefield illumination systems have an almost constant projected spatial frequency or are approximated as such, this endoscopic implementation has a non-negligible monotonic decrease in spatial frequency with increased distance due to the viewing angle of the endoscope (45°). This varying spatial frequency is accounted for by first calibrating over several known distances and then measuring the sample distance at each pixel, as described above. While spatial frequency variation may happen on the sample with varying shape, the "apparent" spatial frequency seen on the CCD does not change. This is paramount because SSOP assumes that the carrier frequency across a row of pixels is constant. This is a very easy assumption to make in most cases, but if the endoscope had a different magnification function for projection and collection, then different distances would have different "apparent" frequencies, and a non-flat sample would cause Fourier filtering issues. For projection and collection, the magnification at a certain distance does not have to be equal - only the rate of change magnification versus distance. This is effectively saying that the angular field of view for projection and collection must be equal.

Much of the data flow follows standard widefield SFDI and SSOP processing implemented on a custom-developed MATLAB code (Mathworks, Natick, MA) that was further adapted for this work. This code has been previously validated in past experiments [11, 16, 19, 20].

Biomedical Optics EXPRESS

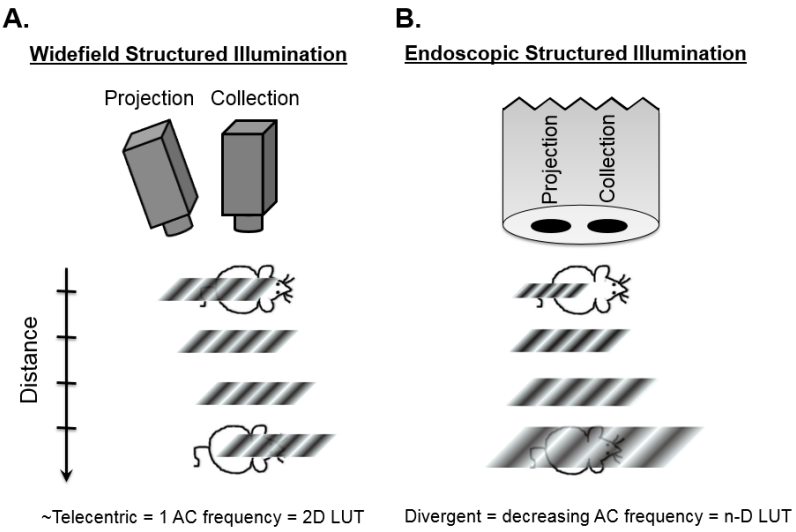

Fig. 3. Schematic demonstrating the projection and collection characteristics (a) a common widefield setup and (b) our endoscopic system. Both systems use the phase shift in the projected sinusoid to measure distance. However, the endoscope system has a field of view dependent on distance, and so this variation is characterized during calibration.

2.5 Calibration

Standard spatial frequency domain imaging requires calibration measurements to generate optical property maps, seen as M_{ref} in Eq. (3) [15]. The calibration phantom used in this experiment was a large (96 x 96 x 20 mm) flat, homogeneous, tissue-mimicking phantom with known optical properties. This calibration phantom was fabricated based on prior work [27], with absorption and scattering parameters adjusted with India ink in polydimethylsiloxane and TiO2, respectively. Two-distance, multifrequency frequency domain photon migration (FDPM) measurements were independently taken to verify the phantom's spectral absorption and scattering properties [28]. The optical properties of this reference phantom were used to calibrate a sample's optical properties, and calibration measurements were made from 4 to 9 cm from the distal end of the endoscope in 1 cm increments to correct for a sample's variation in height. The distance range has been chosen to match the typical working distance of an endoscope. The calibrated parameters (e.g. distance, intensity, spatial frequency) varied slowly enough for low dimensional polynomial fitting, and so 6 calibration points provided a robust fit.

2.6 Experiments

2.6.1 Flat homogeneous phantom

Fixed distance measurement: to first validate the accuracy and precision of extracting optical properties without the involvement of profile correction, a flat, homogeneous, tissue-mimicking phantom with known optical properties was used as a sample and placed at a fixed distance for measurement and calibration. This sample phantom, like the calibration phantom, was fabricated with silicone and used India Ink and titanium dioxide to adjust for absorption and scattering properties, respectively [27]. The sample phantom's known optical properties (μ_a = 0.032 mm^{-1} and μ_s' = 0.99 mm^{-1} as measured by widefield SFDI) were used as gold standards for the measurements made using this endoscopic SSOP system.

Multi-distance measurement: to then validate the system for generating optical property and distance maps over varying distances, the same flat homogeneous phantom was measured at each calibration distance (4 thru 9 cm at 1 cm increments). Validating against the expected

Biomedical Optics EXPRESS

values, distance-based corrected optical property measurements and profile maps were compared with non-corrected optical property measurements for accuracy and precision.

2.6.2 Hemispheric homogeneous phantom

Noncontact clinical endoscopy often images non-flat samples, so this experiment uses a hemispherical tissue-mimicking phantom to assess the profile acquisition and distance-based correction of a curved surface. This silicone phantom was made to have similar optical properties as the flat homogeneous phantom described above by using India Ink and titanium dioxide to control absorption and scattering, respectively (0.025 mm^{-1} and 1.05 mm^{-1}). In order to also test the accuracy of extracted optical properties over time and sample location, a video was acquired of the hemispherical phantom placed on top of the flat homogeneous phantom as it is moved in three dimensions.

2.6.3 *In-vivo* measurement

To demonstrate the endoscopic real-time acquisition of optical properties and profilometry *in vivo*, a video of a hand in motion was taken with the same flat homogeneous phantom as the background.

3. Results

3.1 System design

The optical design shown in Fig. 2(a) has minimal components and can be relatively inexpensive depending on the choice of source, endoscope, and camera. The NIR source used in this system has been built and described in recent work [23]. For this embodiment, we utilized two 1W laser diodes operating at 660 nm (LDX-3115-660, LDX Optronics, Maryville, TN) along with current and thermoelectric cooler controllers (ITC300, Thorlabs, Newton, NJ). The laser module is integrated to the endoscope optical system with a 1 mm multimode fiber optic cable (BFY1000LS02, Thorlabs) and the light is then shaped using two 35 mm focal length biconvex lenses L_1 and L_2 (LB1811, Thorlabs) for illuminating the sinusoidal projection pattern, M. The projection pattern M was printed onto transparency film using an office laser printer. The endoscope used was a dual-imaging, rigid endoscope (Schölly, Inc., Worcester, MA). The projection lens L_3 was a75 mm focal plano-convex lens (LA1765, Thorlabs). A pair of linear polarizers, P_1 and P_2 (PPL05C, Moxtek, Inc., Orem, UT) helped reduce specular reflections on the proximal end of the endoscope. A simple plano-convex objective lens was used for L_4 (#45-508, Edmund Optics, Barrington, NJ) that imaged the sample onto a 14-bit CCD camera (pco.pixelfly usb, PCO, Romulus, MI).

3.2 Flat phantom

Fixed distance measurement: The flat homogeneous phantom was imaged at 6 cm, the same height as the reference phantom (see Fig. 4). At this distance, the field of view of the entire CCD was 5.7 x 7.6 cm. Signal loss towards the edges of the collected image was too low for proper processing, and so a mask (480 pixel diameter circle) was used to remove unusable pixels, slightly decreasing the field of view. Also, close to the mask edge there are apparent artifacts due to this loss of signal, and so all analyzed data was taken from the dotted rectangular ROI (310 x 405 pixels, 3.39 cm x 4.42 cm) in the center of view. Single value reports, like that in Fig. 4, are the statistical mean and standard deviation of the pixels within the ROI for a given image measurement. In Fig. 4(a), the measured absorption of 0.033 ± 0.00037 mm^{-1} was very accurate to the expected value of 0.032 mm^{-1}. Likewise, in Fig. 4(b) the measured reduced scattering 0.96 ± 0.0079 mm^{-1} was very close to its expected value of 0.99 mm^{-1}.

Biomedical Optics EXPRESS

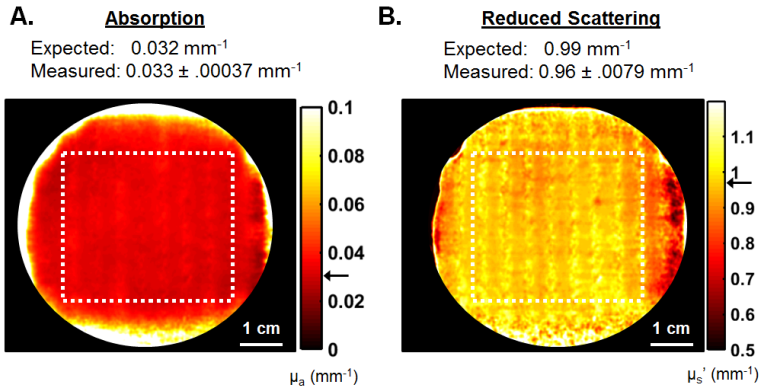

Fig. 4. A flat homogeneous phantom was measured 6 cm from the distal end of the endoscope and (a) absorption and (b) reduced scattering properties were generated. Analysis was done on the white-dotted ROIs. The statistical mean and standard deviation are reported for the set of pixels within the given ROI.

Multi-distance measurement: The flat homogeneous phantom was measured from 4 to 9 cm in 1 cm increments (see Fig. 5). The sample profile maps are shown in Fig. 5(a) with the color showing absorption values. In Fig. 5(b) the measured distance is compared with the known distance of the phantom from the endoscope and shows high accuracy at each distance with a maximum error of 1.3 mm. Each plotted point is the average height within the ROI and includes error bars. In Figs. 5(c) and (d), the uncorrected measurements (blue x's) were referenced against a phantom at 4 cm. The uncorrected measurements lose accuracy rapidly as the sample distance increases, changing by nearly an order of magnitude for absorption and reduced by 0.36 mm^{-1} for scattering. In comparison, the corrected measurements (red squares) show fairly accurate and precise values over the distance range, staying within 0.004 mm^{-1} for absorption and within 0.05 mm^{-1} for scattering.

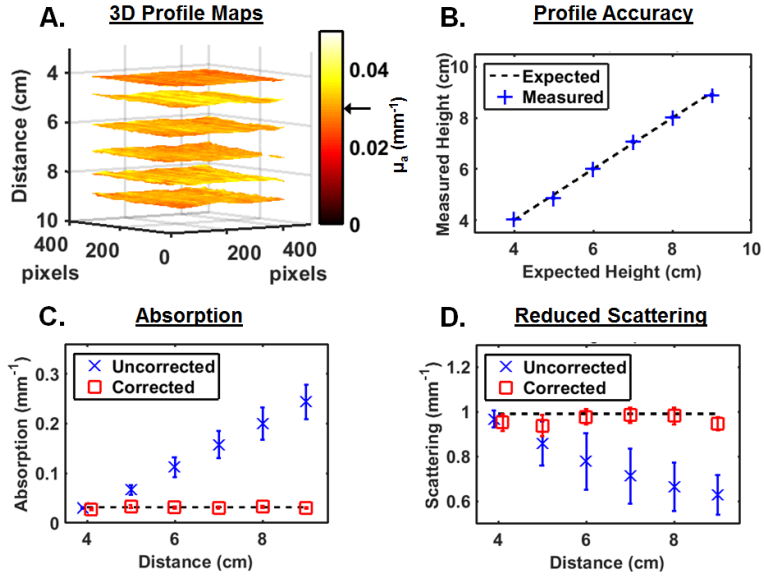

Fig. 5. A flat homogeneous was measured from 4 to 9 cm in 1 cm increments. (a) The surface topography for all 6 measurements are plotted with the color map showing absorption values. (b) The topographical accuracy is shown by analyzing the ROI for each distance measurement. The analyzed (c) absorption and (d) reduced scattering values for the distance-corrected measurement and the uncorrected measurement demonstrate the need for distance-correction.

Biomedical Optics EXPRESS

To demonstrate the general degradation of optical property maps when profilometry is not used, the absorption and reduced scattering maps are presented in corrected and uncorrected formats in Fig. 6. The large color scale range is to capture the large variations in the uncorrected maps. These maps demonstrate not only the large deviation in the average optical properties measured, but also a large increase in standard deviation, with absorption error going from 0.0019 mm^{-1} (corrected) to 0.032 mm^{-1} (uncorrected) and scattering going from 0.048 mm^{-1} (corrected) to 0.13 mm^{-1} (uncorrected). The scale bar given at each height represents 1 cm and demonstrates the correlation between increasing field of view and distance.

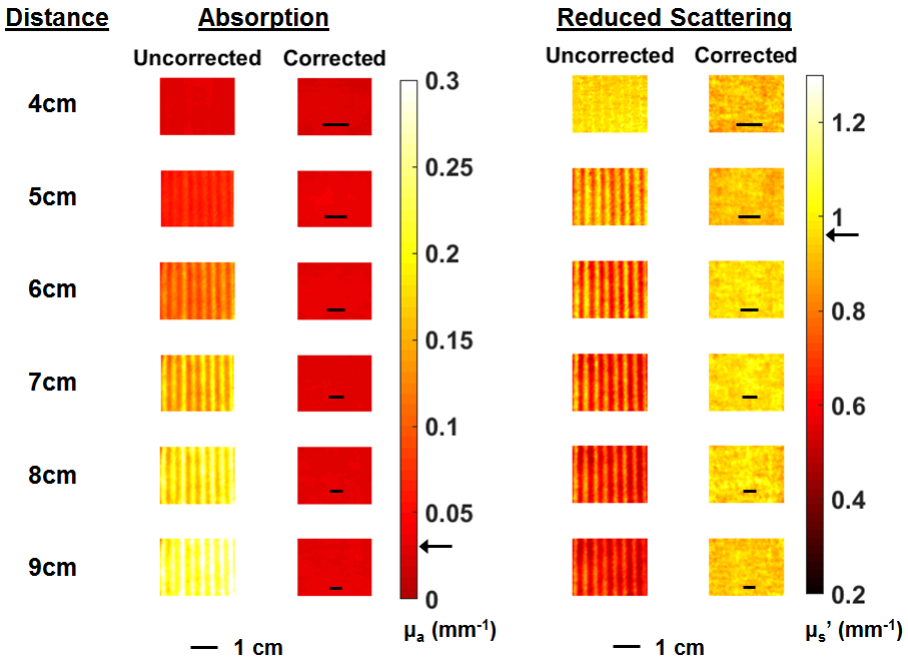

Fig. 6. Absorption and reduced scattering maps measured on a flat homogeneous phantom from 4 to 9 cm. These maps demonstrate the divergence of accuracy when not correcting for sample distance. The arrows on the color bar represent the expected optical property values. The black scale bars represent 1 cm for a given distance. Note the decrease in magnification as distance is increased.

3.3 Hemispheric homogeneous phantom

Figure 7 shows data collected and processed from the real-time acquisition of optical properties for a moving hemispherical phantom and a flat homogeneous background. The video was acquired with a 85 ms exposure time, and thus a framerate of approximately 11 frames per second (fps). The raw data inside the ROI is shown in the upper left frame, and the three extracted measurements of 3D profile (top right), absorption (bottom left), and reduced scattering (bottom right) come from this single raw image. The hemispherical phantom and the flat homogeneous background phantom are translated in the transverse plane in a random manner, showing stable optical property measurements in time and space. The phantom's translation was done by hand, and so slight variations in depth occur. The variations in height mean the field of view is not constant, but a scale bar that represents the scale at a distance of 7 cm is presented. The latter half of the movie captures a large translation in depth and shows stable measurements throughout. Slight optical property artifacts, especially for absorption, occur at the base of the hemispherical phantom and tend to ripple laterally around it.

Biomedical Optics EXPRESS

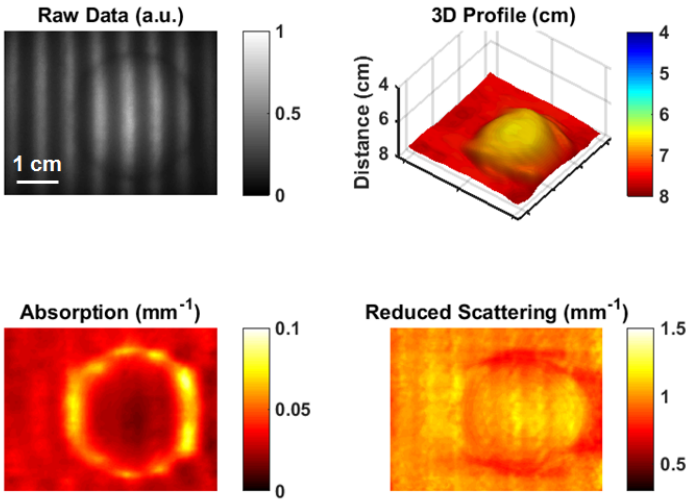

Fig. 7. A hemispherical phantom resting on a flat homogeneous phantom was measured at video rate (~11 fps) (see Visualization 1). Every frame of collected raw data generated a 3D profile, absorption, and reduced scattering maps. Note: since the scale changes with distance, this scale bar is given for 7 cm distance.

3.4 In-vivo measurement

Figure 8 shows the in-vivo experiment with real-time acquisition of optical properties of a hand in motion. In the background is the flat homogeneous phantom previously used, and its position is held constant throughout the experiment. The video was acquired with an 85 ms exposure time (~11 fps), and each ROI frame of raw data (top left) produced the three extracted measurements of 3D profile (top right), absorption (bottom left), and reduced scattered (bottom right). The hand is moved laterally over a static background, showing stable optical property and 3D profile maps throughout. Like Fig. 7, the variations in height mean the field of view is not constant, so a scale bar that represents the scale at 7 cm is presented. Slight optical property artifacts are seen outlining the hand, as well as rippling laterally from the hand.

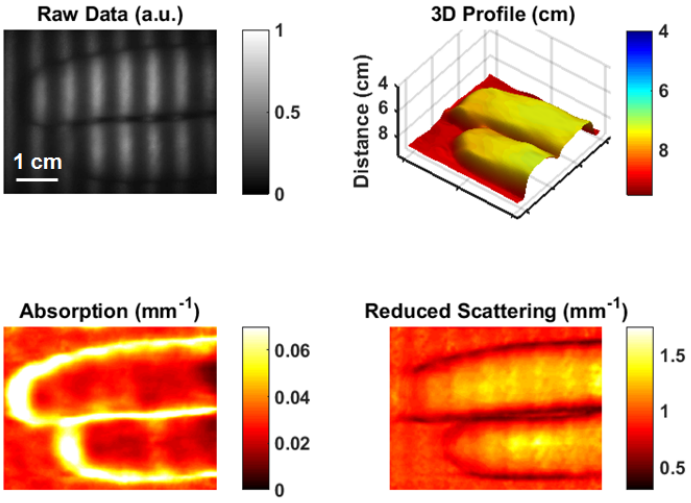

Fig. 8. An *in vivo* sample (hand) is measured at video rate as it passes into view over a homogeneous flat phantom (see Visualization 2).

Biomedical Optics EXPRESS

4. Discussion

In this work, we introduced a novel implementation of single snapshot of optical property (SSOP) imaging capable of acquiring widefield optical property and 3D profile maps in real-time. This technique relies on the projection of a single 1D-sinusoidal illumination pattern that is then imaged and decomposed into components of AC, DC, and phase for further processing in the spatial frequency domain [11, 15, 20]. Calibration at multiple distances is done to calculate optical property and 3D profile maps and to also account for system parameter variations due to changes in the sample distance. The context for this work is focused on enabling quantitative surgical guidance, and while this work demonstrates a benchtop proof-of-concept system toward this goal, several factors should be considered for future work.

During surgery, the field of view is likely to change continuously due to the handling of the endoscope or the *in vivo* sample's motion itself, and so real-time acquisition is crucial to eliminate motion artifacts while imaging. The video framerate demonstrated in these experiments is approximately 11 frames per second, but it should be noted that this technique's framerate is only limited by the time of a single exposure, and so improved throughput and collection efficiency in an optimized system would greatly reduce the exposure time and increase the framerate of this technique. Ideally the acquisition speed would be greater than 15 fps to offer a smooth viewing experience, though cardiac dynamics have been seen in a similar technique done in widefield at rates of 50 fps [29].

Given the intended use of this technique, sample distance variation will most likely be happening continuously during imaging. As shown here, endoscopic SSOP imaging necessitates the use of profilometry correction. As distance is increased, absorption map averages fall by nearly an order of magnitude while reduced scattering was reduced by 0.36 mm^{-1}. Moreover, artifacts become apparent as the measured sample's distance gets farther from the reference phantom's distance (see Fig. 5). The use of profilometry keeps absorption and reduced scattering map averages within 0.004 mm^{-1} and 0.05 mm^{-1}, respectively. Because the single snapshot collects phase information as well, there is no additional acquisition time necessary to measure the sample's phase, though calibration steps are added to create distance-dependent correction factors. Profilometry corrections are therefore necessary for quantitative imaging of samples with variations in height and also help reduce imaging artifacts [16, 17]. These previous studies have also demonstrated an upper limit of 75° for correcting the reflection angle of the sample surface, though further validation is needed for this endoscopic implementation. In the future, phantom studies could further test this technology's robustness by simulating body cavities, potentially by using 3D printing [30].

The spatial information extracted from a single raw image allows for rapid acquisition, but the cost will be some loss of spatial resolution. Figure 4 and the videos presented (Figs. 7 and 8) show a slight loss in image resolution from the raw image collected to the optical property maps, along with minor ringing artifacts due to the demodulation process relying on filtering in the Fourier domain. These artifacts raise concerns for robust quantification and detection during future clinical use, e.g. tumor detection. However, these image degradations tend to be stable and minor in the variations in optical properties. Furthermore, the ability for a high NA endoscope to readily adjust magnification in real-time allows for continuous detailed inspection and contextual referencing. No measure of image quality or viewer experience has been presented in this work because this work is simply a proof-of-concept and a more optimized system will greatly improve image quality. This optimization will mostly entail increased optical efficiency and throughput, along with optimization of SSOP processing framework.

To progress this technique from endoscopic real-time imaging of optical properties to surgical guidance will first entail incorporating a second wavelength in order to enable

Biomedical Optics EXPRESS

oximetry imaging. Previous work has demonstrated the ability of spatial frequency domain imaging to perform accurate oximetry measurements in tissue with only two wavelengths [18], making endoscopic real-time oximetry imaging readily achievable by adding a second wavelength to the benchtop system presented here. The next concern will be to perform real-time acquisition along with real-time feedback. Two fundamental hurdles need to be considered: 1) demodulation time and 2) inversion of measured diffuse reflectance to sample properties, e.g. optical property or chromophore maps. Demodulation time is currently estimated at 100 ms, though this processing is currently being done in MATLAB and could certainly be optimized for real-time feedback. While the current processing time to invert diffuse reflectance maps to optical properties is typically on the order of 1 second, we recently demonstrated that this inversion time could be reduced significantly to approximately 10 ms [31]. Altogether this work lays the foundation of real-time quantitative optical imaging through an endoscope and its clinical translation, potentially enabling endoscopic implementation of current quantitative, widefield techniques [32–34].

5. Conclusion

The endoscopic SSOP system allows for real-time imaging of profile-corrected optical properties through an endoscope. In this work, we presented the principles and methods of this system's design and processing scheme, along with a validation of its accuracy on tissue mimicking phantoms and a demonstration of its *in-vivo* imaging capabilities. In addition, the method presented is also capable of measuring the sample profile and corrects for variations in the sample's distance from the endoscope to obtain accurate optical property maps from a single image acquisition with a slight loss in image resolution. This work utilizes previous investigations into widefield imaging of optical properties to lay the foundation for real-time, endoscopic surgical image-guidance using endogenous contrast.

Funding

National Institutes of Health (NIH) (K01-DK-093603, F31-DK-105839); European Research Council (ERC) (715737); France Life Imaging; University of Strasbourg IdEx and ICube Laboratory.

Acknowledgments

The authors would like to thank Intuitive Surgical and Jonathan Sorger for their support with instrumentation.

Disclosures

The authors declare that there are no conflicts of interest related to this article.

130.79.74.79 {ts '2017-10-23 03:55:25'}